RSC Advances

ROYAL SOCIETY OF CHEMISTRY

www.rsc.org/advances

Polyphenylsulfone-based solvent resistant nanofiltration (SRNF) membrane incorporated with copper-1,3,5-benzenetricarboxylate (Cu-BTC) nanoparticles for methanol separation

N.A.A. Sani, W.J. Lau, A.F. Ismail*

Advanced Membrane Technology Research Centre (AMTEC), Universiti Teknologi Malaysia, 81310 Skudai, Johor, Malaysia
*Corresponding author: afauzi@utm.my; fauzi.ismail@gmail.com
Tel: +607 553 5592; Fax: +607 558 1463

Abstract

Mixed matrix membranes (MMMs) of various properties were prepared for solvent resistant nanofiltration (SRNF) process by incorporating polyphenylsulfone (PPSU) membranes with self-synthesized copper-1,3,5-benzenetricarboxylate (Cu-BTC) nanoparticles at different loadings. Cu-BTC nanoparticles were homogeneously dispersed in PPSU dope solution prior to casting process, and their subsequent presence in the PPSU membrane was inferred by a combination of FTIR spectroscopy, TGA, SEM, EDX and AFM analyses. These analyses confirmed the existence of Cu-BTC particles and their distribution pattern in the membrane matrix. Membrane performance in organic solvent nanofiltration was evaluated on the basis of methanol permeance and dyes-methanol separation. Results showed that membrane pure methanol flux was significantly improved from 102 L/m^2.h in the pristine PPSU membrane to >135 L/m^2.h in the membrane incorporated with 3 wt% Cu-BTC into PPSU membrane when both membranes were tested at 14 bar. Apart from preferential channels created by Cu-BTC, the existence of interfacial voids in MMMs also contributes to the flux improvement owing to the formation of alternative paths for solvent transportation. Results also showed that the membranes incorporated with low loadings of Cu-BTC (ranging between 0.5 and 1.0 wt%) tended to have smaller molecular weight cut-off (MWCO) than that of pristine PPSU and PPSU incorporated with 3 wt% nanoparticles, leading to smaller surface pore size but better separation efficiency. The improvement on membrane flux and dyes rejection at low Cu-BTC loadings could be attributed to the good dispersion of the nanoparticles in the membrane matrix coupled with their improved interfacial contact with the membrane. The newly developed membrane also showed a great improvement in terms of resistance to compaction, suggesting Cu-BTC particles is of importance in increasing membrane rigidity and strength.

Keywords: Solvent resistant nanofiltration; mixed matrix membranes; metal organic frameworks

1.0 Introduction

Solvent resistant nanofiltration (SRNF) is a relatively young membrane separation technology that broke through around the beginning of this century. SRNF-based technology has been proven to be significant in expanding the spectrum of membrane applications from aqueous systems primarily for water purification and other water-related treatments to filtration and concentration of non-aqueous solutions. This relatively new technology holds enormous potential as it allows separation of small compounds with molecular weight (MW) ranging from 200 to 1400 Da from organic solvents. The possible industrial applications of SRNF-based technologies include recovery of solvent in lube oil dewaxing processes [1], degumming of vegetable oil [2], reuse of extraction solvent in the food industry [3] and purification of active pharmaceutically ingredients (API) [4].

The most commonly used membranes for SRNF applications are asymmetric polymeric membranes which typically consist of a dense selective layer on the top of microporous structure. This asymmetric configuration is further deduced as: (a) the integral type, where the entire membrane is composed of the same polymeric material and (b) the thin-film composite (TFC), where the membrane separating layer is made of a different material. Polymeric membranes derived from polyimide (PI) [5, 6], polyamide (PA) [7], polyacrilonitrile (PAN) [8], polyphenylsulfone (PPSU) [9, 10] and polypyrrole (PPy) [11] have been previously used for the SRNF applications. Details about these polymeric materials as well as their structures could be found in two review articles written by Vandezande et al. [12] and Cheng et al. [13] in 2008 and 2014, respectively. Membranes made of polymeric materials have the advantages of being inexpensive for fabrication process and easy to scale-up. They have gained popularity due to their potential in a wide range of applications but flux decline over time resulted from membrane compaction and/or fouling problem is always the main concern to many. Furthermore, most of the polymeric membranes show relatively low thermal and chemical stability when tested in aggressive condition [14]. Several strategies have been attempted to overcome these problems, for instance improving membrane surface properties by chemical modification method [15] or incorporating pristine membrane with secondary polymeric material/inorganic nanoparticles [5, 7, 16].

The advent of new type membrane so-called mixed matrix membrane (MMM) has received enhanced attention recently. This membrane type was originally developed for gas separation processes [17, 18]. They are formed by embedding appropriate amount of inorganic nanoparticles into membrane

matrix. Both the polymer (membrane) and inorganic fillers could be connected via covalent bonds, van der Waals forces or hydrogen bond to produce membranes with desirable chemistries. An investigation of MMM for SRNF application was first reported by Gevers et al. [19] in 2005 using silica, carbon and zeolites as fillers for polydimethylsiloxane (PDMS)-based membranes. They found that the zeolites-filled PDMS was an excellent SRNF membrane as this membrane exhibited enhanced fluxes and rejections compared to the PDMS membranes incorporated with silica and carbon fillers. Soroko and Livingston [5] on the other hand reported the performance of titanium dioxide (TiO_2)-filled PI membranes in pure solvents (N,N-dimethylformamide (DMF) and ethanol) and styrene oligomer-solvent mixtures. The experimental results that the membrane compaction resistance was improved significantly with separation performance remained unchanged upon addition of 10 wt% TiO_2. This findings show that TiO_2 is capable of improving membrane mechanical properties by preventing membrane porous structure from collapsed. Siddique et al. [20] in recent year prepared inorganic organosiloxane/PI MMMs for API purification. The performance of the MMM was compared with the commercially available membrane (Duramem™ 300, Evonik Membrane Technology Ltd, UK) and the results show that the in-house made MMMs were more resistant against pressure compaction (tested at pressure up to 30 bar), although a lower solvent flux was recorded.

Previous research works have shown that to certain extent the introduction of inorganic fillers into membrane matrix could improve solvent flux and/or enhance mechanical stability, but poor adhesion between polymer and inorganic filler is likely to occur which may result in interface void formation. These voids, that are much larger than solute size, may negatively affect membrane rejection rate. Therefore, metal organic framework (MOF) has been proposed in this work for MMMs fabrication with the aim of minimizing formation of void as well as flux decline. MOF is a porous crystalline material constructed from metal ions/clusters and multidentate organic linkers [21]. The use of MOFs in MMMs could offer potential advantages over other nanostructured porous materials mainly due to the better affinity of organic linkers of MOFs towards polymer chains [22]. Recent developments have shown the promising applications of MOFs as gas storage, adsorbents for separations drug delivery carriers and catalysts [23-25]. Since the size, shape and chemical functionalities of the MOF cavities can be easily adjusted by choosing appropriate linker-metal couples, MMMs incorporated with MOFs have been widely used in gas separation processes [26-28]. Of the various MOFs available, $Cu_3(BTC)_2$ (herein referred to as Cu-BTC) was selected in this work as it is one of the most studied MOFs since its first research article published in 1999 [29]. Cu-BTC contains two copper ions

forming a Cu-Cu bond at the center of the cluster and connecting four pairs of carboxylates to build a 3D network with nanoscale channels (0.9 nm × 0.9 nm) [30, 31]. These unique channels are suitable to transport most solvents used in SRNF and are capable of rejecting solute of a certain size. For instance, non-aromatic solvents (methanol, ethanol, isopropanol and methyl ethyl ketone) have small kinetic diameters in the range of 0.4–0.5 nm which can adsorb into the Cu-BTC channels, reducing its transport resistance [32].

Despite the excellent properties of Cu-BTC, only a few research groups have studied about Cu-BTC nanoparticles for SRNF application. Basu et al. [33] prepared MMMs using several types of MOFs such as Cu-BTC, MIL-47, MIL-53(Al) and ZIF-8 as dispersed phases in PDMS membranes. According to them, the incorporation of MOFs (except ZIF-8) in the PDMS membrane was able to improve dye rejection (Rose Bengal, MW = 1018 g/mol) from 87% (in pristine PDMS) to 95-98% in isopropanol, owing to the reduced polymer swelling and improved size exclusion effect upon filler incorporation. Campbell et al. [34] prepared Cu-BTC/PI membranes by adding $Cu_3(BTC)_2$ in the PI dope solutions. The performance of the membrane was later tested in polystyrene (PS)-acetone mixtures and compared with the control PI membrane. They found that the prepared MMM showed higher PS rejections and lower flux decline than the control membrane. It is suggested that the addition of Cu-BTC could change the transport properties of the membrane and provide a rigid support to the entire membrane structure.

In view of the advantages of Cu-BTC on MMM performance, efforts will be made in this work to introduce Cu-BTC into new member of the polysulfone (PSF) family, which is polyphenylsulfone (PPSU) in order to further improve solvent fluxes PPSU-based SRNF membrane, without sacrificing solute rejection. As shown in Figure 1, the PPSU which comprises sulfone moieties, ether linkages and biphenyl group in its repeat group presents superior resistant to hydrolysis and plasticization of stress cracking compared with the other family members such as PSF and polyethersulfone (PES) [35, 36].

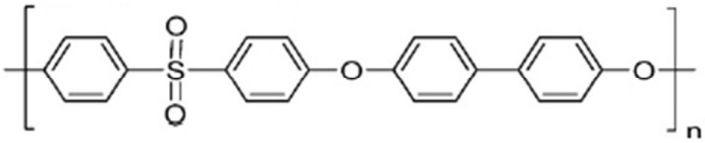

Figure 1: Chemical structure of polyphenylsulfone.

This is the first study reporting the incorporation of self-synthesized Cu-BTC (at various loadings) into PPSU matrix for the separation of methanol-dye mixtures. Cu-BTC was synthesized at room temperature using

copper nitrate and 1,3,5-benzenetricarboxylic acid and was characterized using different instruments. Prior to solvent filtration experiments, the prepared PPSU/Cu-BTC MMMs were characterized with respect to structural, chemical, thermal and mechanical properties. Dyes with MW in the range of 269–1470 g/mol were used to determine separation performance of membrane made of different Cu-BTC loadings. At last, flux stability test of the MMM was also carried out and further compared with control PPSU membrane.

2.0 Experimental

2.1 Materials

PPSU polymer pellets with MW = 50,000 g/mol and specific gravity of 1.29 (Radel R-5000 NT) was purchased from Solvay Advanced Polymers, United States. Solvents ((N-methyl-2-pyrrolidinone (NMP) and dimethyl sulfoxide (DMSO)) used to prepare membranes and synthesize Cu-BTC as well as for filtration experiments (methanol) were obtained from Merck, Malaysia and were all in analytical grade (purity >99%). Copper nitrate trihydrate ($Cu(NO_3)_2.3H_2O$) and 1,3,5-benzenetricarboxylic acid (trimesic acid) used for Cu-BTC synthesis were purchased from Sigma-Aldrich, Malaysia. Methyl red (MR), reactive orange 16 (RO16), methyl blue (MB), and reactive red 120 (RR120) purchased from Sigma-Aldrich, Malaysia were used for solute rejection experiments by dissolving them in methanol solution. The MW of dyes in methanol solution together with their maximum absorption wavelength is summarized in Table 1.

Table 1: Molecular weight and maximum adsorption wavelength of selected dye compounds

Dye	Molecular weight (g/mol)	Maximum absorption wavelength (nm)
Reactive Red 120 (RR120)	1470	539
Methyl Blue (MB)	800	316
Reactive Orange 16 (RO16)	616	494
Methyl Red (MR)	269	496

2.2 Synthesis of Cu-BTC

Cu-BTC was synthesized according to the procedure described elsewhere [37]. A precursor solution was prepared by dissolving 1.22 g $Cu(NO_3)_2.3H_2O$ and 0.58 g trimesic acid in 5 g DMSO as shown in step (A)1 of Figure 2. The solution was then stirred for 2 h at room temperature. 4

mL ethanol was then carefully layered on the top of 0.5 mL precursor solution in a glass vial (step (A)2). After 24 h, the precipitate settling at the bottom was collected by centrifugation and washed twice with pure ethanol (step (A)3). At last, the nanoparticles were dried overnight in oven at 70°C in order to produce dry Cu-BTC powder ((A)4).

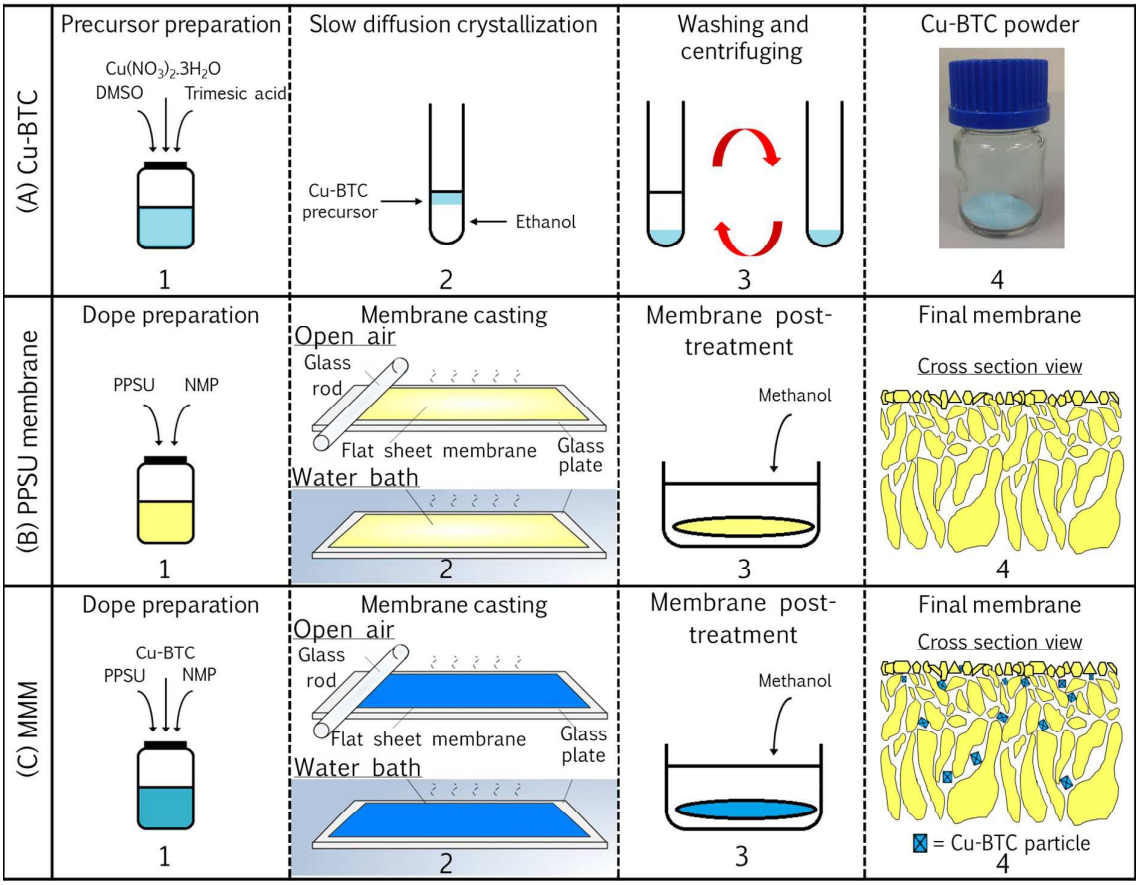

Figure 2: Schematic of (A) Cu-BTC synthesis, (B) control PPSU membrane and (C) MMM processes.

2.3 Membrane preparation

2.3.1 Preparation of polyphenylsulfone (PPSU) membrane.

Integrally skinned asymmetric PPSU membrane was prepared via a phase inversion method. A dope solution was formed by dissolving 17 wt% of polymer pellets in NMP solvent as shown in step (B)1 of Figure 2. The PPSU and the NMP was stirred at least 20 h in a sealed container to ensure no moisture was absorbed into the dope solution. The dope solution was left for 24 h to remove any entrapped air bubbles. The dope solution was cast onto a glass plate without any non-woven support using a glass rod at room

temperature. Immediately after casting, the membrane was immersed in a water bath where phase inversion occurred (step (B)2). After 15 min, the membrane was placed in a fresh water bath and left for 24 h to ensure sufficient removal of solvent and stability of the membrane final structure. Lastly, the membrane was air-dried for 24 and kept in dry air-tight container. Prior to any analyses, the membrane was conditioned with methanol for 5 min (step (B)3).

2.3.2 Preparation of PPSU/Cu-BTC mixed matrix membrane.

MMM was prepared from the solution consisting of PPSU, NMP and Cu-BTC. Cu-BTC nanoparticles at loadings of 0.5, 0.8, 1 and 3 wt% based on the total weight of PPSU/NMP (17/83) dope solution were first dispersed in NMP solvent before adding polymer pellets (step (C)1 of Figure 2). After polymer dissolution was complete, the Cu-BTC solution was added and stirred until the solution became homogeneous. The dope solution was placed in an ultrasonic bath for 1 h to prevent agglomeration of the particles, and then left overnight to disengage air bubbles. The MMM was produced by immersing as-cast film in water (step (C)2). Lastly, the membrane was air-dried for 24 h and kept in dry air-tight container. Similar to control PPSU membrane, all MMMs were conditioned with methanol for 5 min (step (C)3) prior to any analyses. PPSU/Cu-BTC MMMs with 0.5, 0.8, 1 and 3 wt% Cu-BTC loading were hereafter denoted as PPSU/0.5Cu-BTC, PPSU/0.8Cu-BTC, PPSU/1Cu-BTC and PPSU/3Cu-BTC, respectively.

2.4 Membrane characterization

2.4.1 Transmission electron microscopy

The Cu-BTC particle size and distribution was determined by transmission electron microscopy (TEM) using Philips CM12 (Philips, Eindhoven, The Netherlands) operated at 80 kV. The sample is carefully single-dropped on a tiny 400 mesh copper grids after being diluted in water. The images were captured by an SIS image Analysis V3.11.

2.4.2 X-ray powder diffraction

The X-ray powder diffraction pattern was acquired at room temperature with a diffractometer (Siemens D5000, Siemens AG, Germany) equipped with a graphite monochromatized Cu-kα radiation ($\lambda = 1.5418$Å). The data was collected between 5° and 20° angular range in 2θ in continuous scan mode using a step size of 2° and a step time of 1 min.

2.4.3 Fourier transform infrared spectroscopy

Fourier transform infrared (FTIR) spectra were recorded on a Nicolet 5700 (Thermo Electron Scientific Instruments Corporation, USA). The spectra were collected in the attenuated total reflection (ATR) mode. The spectra were recorded in the 4000–600 cm^{-1} wavenumber with an average of 16 scans and at a resolution of 4 cm^{-1}.

2.4.4 Thermogravimetry analysis

The thermal stability was investigated by thermogravimetric analysis using Mettler Toledo thermogravimetric analyser (TGA) (TGA/SDTA851, USA). The samples were heated from 30 to 800°C under a nitrogen atmosphere with at a heating rate of 10°C/min. Experiments were performed on samples with an average mass of 5 mg, using a purge gas flow rate of 20 mL/min.

2.4.5 Mechanical strength test

Tensile strength and elongation at break of the membranes were measured using an LRX 2.5 SKN (Lloyd Instruments, Ltd., US), by employing a deformation speed of 10 $mm.min^{-1}$ at room temperature. Three membranes of each type were tested and the average results were reported.

2.4.6 Scanning electron microscopy/energy-dispersive X-ray spectroscopy

The surfaces and cross-sections of the membrane were examined by scanning electron microscopy (SEM) and elemental analysis of the membrane samples was conducted using energy-dispersive X-ray (EDX) spectroscopy. For the sample preparation, the membranes were immersed in liquid nitrogen and fractured carefully to have a clean brittle. The samples were mounted on carbon tape and coated with platinum-coated using a sputter coater to avoid surface charging during analysis. The microscopic analyses were performed using scanning electron microscope (TM3000, Hitachi, Japan) equipped with an EDX spectrometer (XFlash® 430H Detector, Bruker).

2.4.7 Atomic force microscopy

The atomic force microscopy (AFM) measurement for membrane surface morphology was carried out using a Multimode Nanoscope (Digital Instruments Inc., Santa Barbara, CA, USA). The roughness of membrane surfaces was obtained from the AFM images using NavoNavi Station software (version 5.01C). The surface roughness was expressed by a root-mean-square

roughness (R_q) – average of height deviations taken from the mean data plane: $R_q = \sqrt{(Z_i^2/N)}$ where Z is the peak-to-valley difference in height values within the analysed region. The scanning area of each membrane was 10 μm × 10 μm.

2.5 SRNF experiments

The experiments were performed using a stainless steel dead-end stirred cell (Sterlitech HP4750, Sterlitech Corporation, USA). A nitrogen cylinder equipped with a two-stage pressure regulator was connected to the top of the stirred cell to supply desired pressure. The operating pressure was controlled at between 6 and 14 bar for pure methanol flux measurement and 6 bar for all other filtration experiments. In order to minimize concentration polarization during the experiment, Teflon-coated magnetic stirring bar was used and controlled at 1200 rpm on top of the active side of membrane. Membrane circular coupons were of 14.6 cm^2 (effective diameter: 4.3 cm). Prior to the filtration experiments, the membranes were compacted at pressure of at least 7 bar for about 1 h. The membrane flux was collected when flux had achieved steady-state and was measured every 10 min for up to 2 h. For methanol flux stability test, the experiment was paused after every 1 h of running in order to top up the stirred cell with methanol solvent. The flux, J ($L/m^2.h$) of membrane was determined by measuring volume of permeate (V) per unit area (A) per unit time (t) according to the following equation:

$$J = \frac{V}{A\Delta t} \tag{1}$$

With respect to dye rejection determination, the experiment was carried out by filtering methanol solution containing single dye compound (see Table 1) at initial dye concentration of 10 mg/L. The rejection rate, R (%) of the dyes by the membranes was calculated using the following equation:

$$R\,(\%) = \left(1 - \frac{C_p}{C_f}\right) \times 100 \tag{2}$$

where C_p is the dye concentration of permeates and C_f is the initial concentration. Concentrations of permeate and feed solutions were measured using UV-vis spectrophotometer (DR5000, Hach Company, USA). Blank wavelength scan with pure methanol was first performed prior to permeate sample analysis.

3.0 Results and Discussion

3.1 Characterization of Cu-BTC nanoparticles

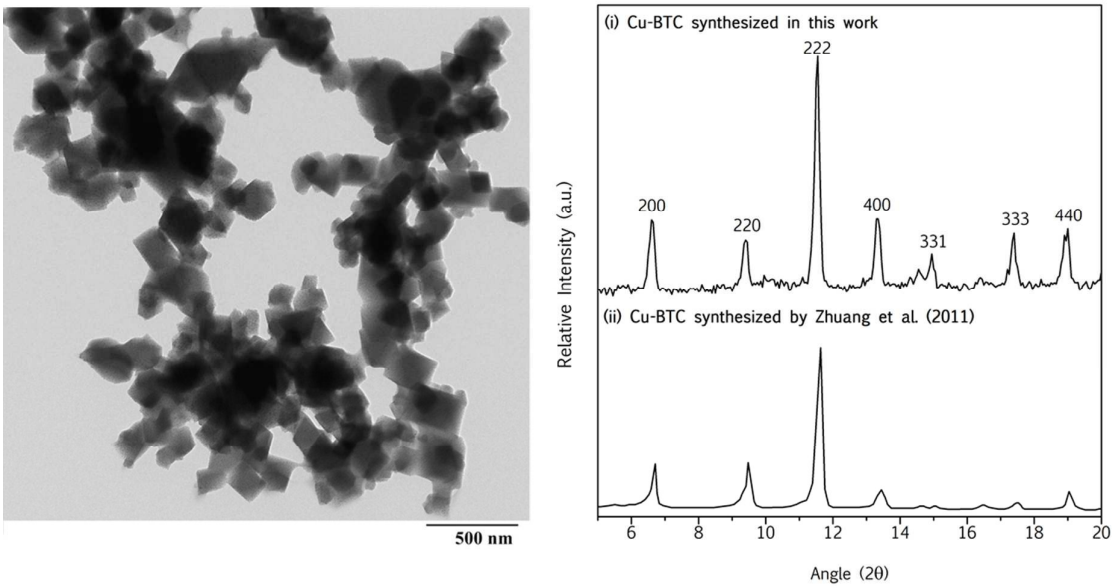

(a) (b)

Figure 3: Characterization of Cu-BTC; (a) TEM image (scale bar: 500 nm) and (b) XRD pattern (compared with other work).

Figure 3(a) shows the TEM image of the Cu-BTC synthesized at room temperature. A distinct cubic crystalline structure and particle size of around 200–300 nm is observed. It should be noted that the size of nanoparticles (in nanometer range) is of importance to reduce membrane surface defects during fabrication process. Figure 3(b) shows the XRD pattern of the Cu-BTC with their corresponding hkl. The results are further compared with the nanoparticles synthesized by Zhuang et al. [37] in which both nanoparticles exhibit similar structural properties, recording sharp peaks at 2θ of 6.6°, 9.4°, 11.5°, 13.3°, 17.2° and 18.9°.

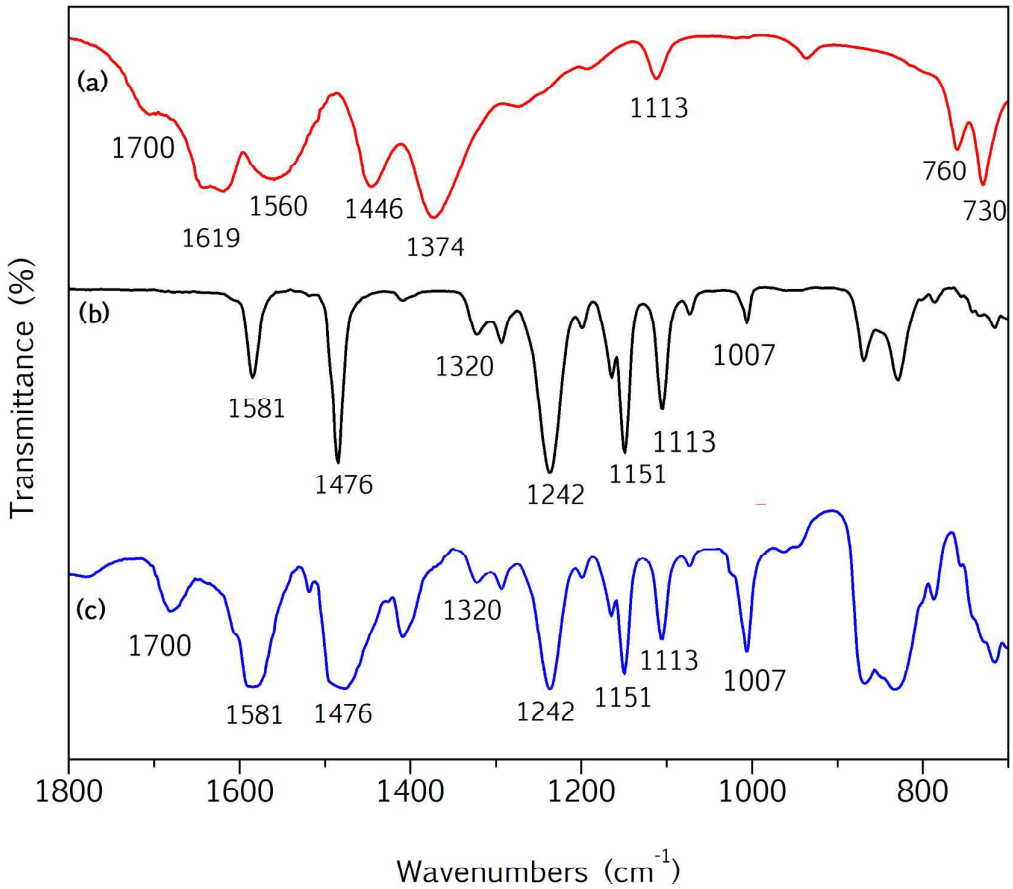

Figure 4: FTIR spectra of (a) Cu-BTC nanoparticles, (b) PPSU membrane and (c) PPSU/0.8Cu-BTC in the characteristic wavenumber ranges.

Figure 4 compares FTIR spectra of as-synthesized Cu-BTC particles and PPSU membrane embedded with and without Cu-BTC. In Figure 4(a), the band at around 1700 cm^{-1} which related to the carboxylate ligands is the sign of coordination of BTC to the copper site [38]. The band at 1619 cm^{-1} is attributed to the H–O–H banding vibration, which indicates that Cu-BTC contains crystal water. The band at 1560 cm^{-1} represents the asymmetric stretching vibrations of the carboxylate groups in BTC, while those at 1446 cm^{-1} are for the symmetric stretching vibrations [38]. The band at 1113 cm^{-1} indicates C–O–Cu stretching of Cu-BTC nanoparticles. The bands at 730 and 760 cm^{-1} are attributed to metal Cu substitution on benzene groups, which can be regarded as the characteristic bands of Cu-BTC. The presence of these characteristic peaks provides clear evidence of the successful synthesis of Cu-BTC.

TGA analyses for Cu-BTC nanoparticles, PPSU membrane and PPSU/0.8Cu-BTC membrane are shown in Figure 5. Three steps of weight loss are noted for Cu-BTC nanoparticles. The first two weight loss steps, at about 75°C and 290°C are corresponded to the physically and chemically absorbed water in the Cu-BTC structure, respectively. The third step at about 370°C is corresponded to the removal of the organic linker and decomposition of Cu-BTC structure.

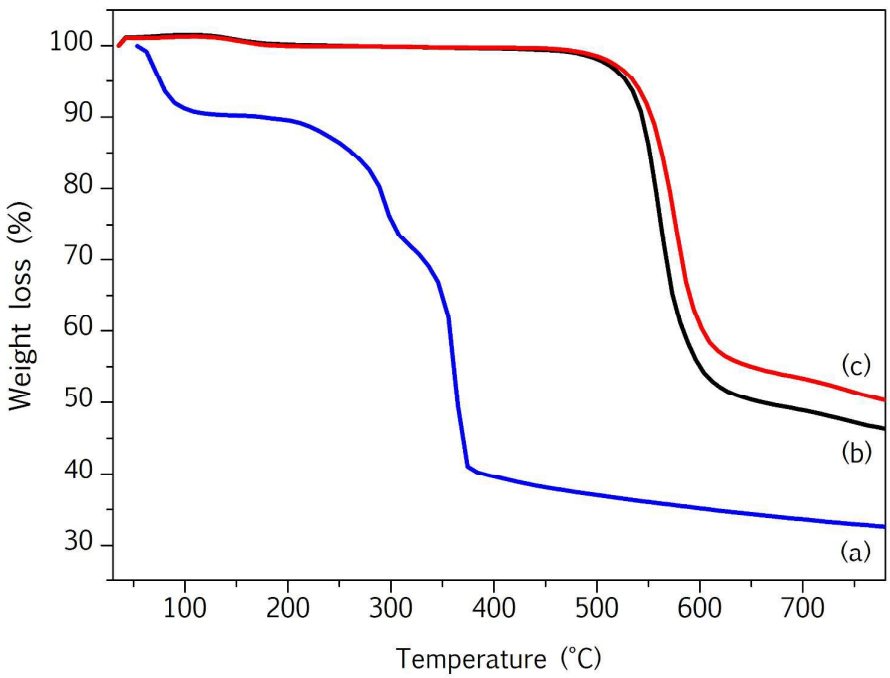

Figure 5: TGA curves for (a) Cu-BTC nanoparticles, (b) PPSU membrane and (c) PPSU/0.8Cu-BTC membrane.

3.2 Characterization of asymmetric PPSU and PPSU/Cu-BTC mixed matrix membranes

The FTIR spectrum of PPSU membrane and PPSU/0.8Cu-BTC membrane are compared and the results are shown in Figure 4(b) and (c). In Figure 4(b), the PPSU shows absorption peaks at 1320 and 1151 cm^{-1} which can be ascribed to the asymmetrical and symmetrical stretching vibrations of the SO_2 group, respectively. The sharp peaks at 1581 and 1476 cm^{-1} arise from the C-C stretching of the aromatic rings and that at 1242 cm^{-1} is related to the C-O stretching vibration of the ether group. In addition, the band at 1113 and 1007 cm^{-1} are assigned to the symmetric and asymmetric stretching of the S=O group [39]. Results show most of the peaks appeared in

PPSU could also be found in the PPSU/0.8Cu-BTC (Figure 4(c)). As only a small amount of Cu-BTC is used in MMM making, the characteristic bands of the nanoparticles are rather weak in membrane matrix. However, the strong band observed at 1700 cm^{-1} could suggest the existence of carboxylate group in the organic ligands of Cu-BTC. Since the C–O–Cu band is masked by the S=O stretching of PPSU, its peak at 1113 cm^{-1} is not well pronounced. In summary, the FTIR results suggested that there is no strong chemical bonding between PPSU and Cu-BTC, the presence of nanoparticles in membrane matrix is mainly based on physical interaction.

With respect to thermal properties, the PPSU membrane (Figure 5(b)) exhibits a single distinct degradation that initiates (T_i) at 502.3°C and shows the maximum rate of weight loss (T_{max}) at about 566°C. Single step decomposition is also observed for the PPSU/0.8Cu-BTC membrane (Figure 5(c)), albeit shifted to higher temperature. Table 2 summarizes the detailed degradation temperature of all MMMs prepared in this work. At the highest Cu-BTC loading (3 wt%), the increases in T_i and T_{max} by around 11 and 18°C, respectively suggest the thermal stability of the MMM is improved upon Cu-BTC incorporation. This improvement is attributed to the formation of a Cu-BTC network that strongly interacts with the matrix and restricts the thermal motions of the chain segments [39].

Table 2: Thermal parameters obtained from TGA analysis for PPSU and MMMs.

Membrane	^aT_i (°C)	$^bT_{10}$(°C)	$^cT_{max}$(°C)
PPSU	502.3	542.5	565.5
PPSU/0.5Cu-BTC	495.0	547.2	572.2
PPSU/0.8Cu-BTC	494.2	550.0	573.0
PPSU/1Cu-BTC	509.3	553.0	578.7
PPSU/3Cu-BTC	513.2	557.2	581.2

^aT_i: Initial degradation temperature obtained at 2% weight loss
$^bT_{10}$: Temperature for a 10% weight loss
$^cT_{max}$: Temperature for a maximum rate of weight loss

Figure 6 shows the tensile strength and elongation at break of the prepared PPSU and PPSU/Cu-BTC membranes. In comparison to PPSU membrane, it is found that the membrane incorporated with 0.8 wt% Cu-BTC could improve membrane tensile strength by as much as 29%. The degree of mechanical properties is further improved to 76% with the introduction of 1 wt% into PPSU membrane matrix. The improved mechanical properties can

be attributed to the well distribution of Cu-BTC nanoparticles throughout the polymer matrix. Excessive use of Cu-BTC (3 wt%) however negatively affects membrane mechanical properties as evidenced in PPSU/3Cu-BTC membrane. This is likely due to the agglomeration of nanoparticles which act as stress concentrator [40, 41].

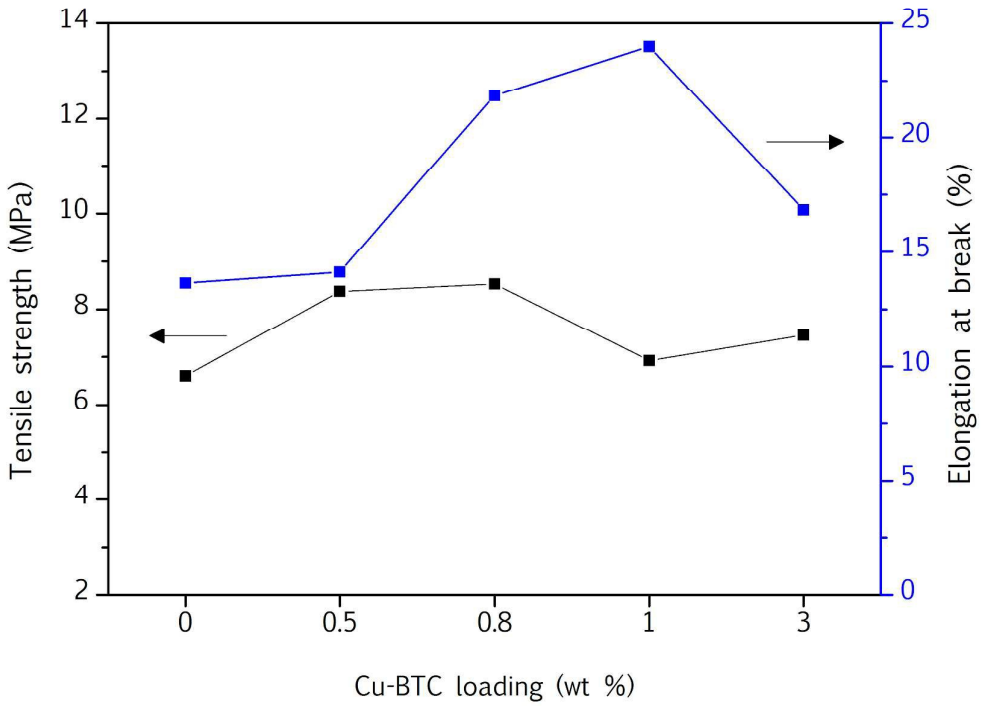

Figure 6: Tensile strength and elongation at break of PPSU-based membrane as a function of Cu-BTC loading.

Figure 7 presents the SEM images of the cross sectional structure and top surface of the PPSU-based membrane incorporated with different Cu-BTC loading. The cross section of all prepared membranes shows a typical asymmetric structure. The PPSU membrane (Figure 7(a)) displays a dense structure in the top layer, finger-like in the sub-layer and macrovoids in the bottom layer. However, with the presence of the Cu-BTC particles in the PPSU matrix, the finger-like structure has been diminished as can be seen from Figure 7(b)-(e). This phenomenon can be related to the increased viscosity of the polymer dope solution as shown in Table 3. It is proved by many researchers that increasing viscosity may work as a void-suppressing factor, as it slows down the exchange rate of solvent/non-solvent, shifting the path of phase inversion from instantaneous into delayed liquid-liquid demixing[10, 42-44]. In addition, formation of bigger macrovoids can be observed

at the bottom layer of the membranes incorporated with higher Cu-BTC loading (Figure 7(d) to (e)). During a phase inversion process, the membrane was easily peeled off from the glass plate which provoked the phase inversion occurred from the bottom layer. Referring to the membrane surface, a random Cu-BTC particles (red circle) distribution can be observed on the surface of MMMs. However, the addition of highest Cu-BTC loading (3 wt%) could lead to significant agglomeration as shown in Figure 7(e).

Furthermore, in order to investigate the dispersion quality of Cu-BTC particles, the EDX analysis was also performed on the active layer of the PPSU/0.8Cu-BTC membrane. The copper (Cu) signal is used to show the distribution of Cu-BTC in the membrane. The height of the red lines in Figure 8 reflects the relative 'counts' of Cu across the active layer (shown in yellow line) of the membrane. From the results, it can be confirmed that Cu-BTC particles are well-distributed throughout the PPSU matrix.

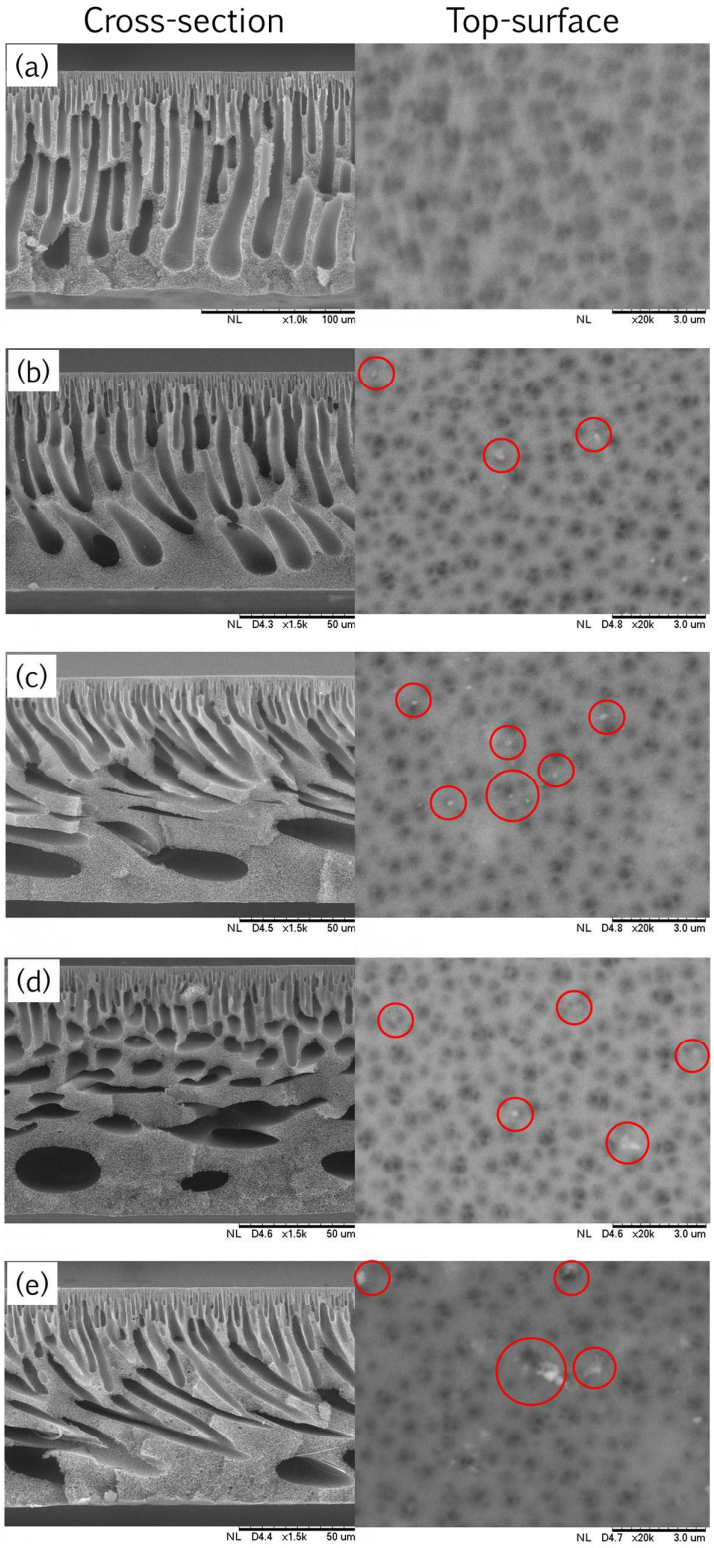

Figure 7: SEM images of cross section and top surface of PSSU membranes embedded with different Cu-BTC loadings (a) control PPSU, (b) 0.5 wt%, (c) 0.8 wt%, (d) 1 wt% and (e) 3 wt%.

Table 3: Effect of the Cu-BTC particles on the viscosity of dope solutions

Membrane	Viscosity dope solution (mPa.s)
PPSU	1,168.6 ± 1.2
PPSU/0.5Cu-BTC	1,224.5 ± 0.8
PPSU/0.8Cu-BTC	1,295.7 ± 0.8
PPSU/1Cu-BTC	1,381.3 ± 0.9
PPSU/3Cu-BTC	1,456.6 ± 1.1

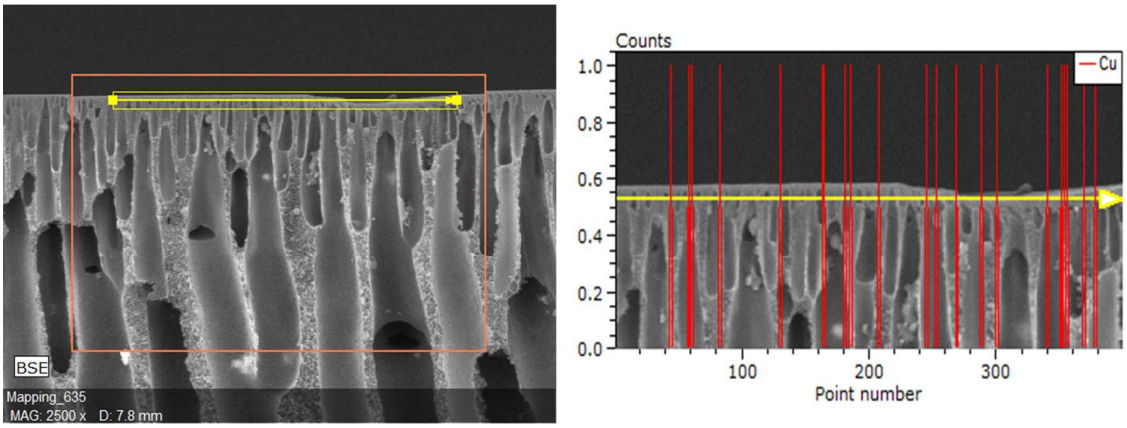

Figure 8: SEM/EDX images of the cross-section of PPSU/0.8Cu-BTC membrane

Figure 9 illustrates three-dimensional AFM images of the surface [4 μm × 4 μm] of the prepared membranes. The brightest regions represent the highest peak of the membrane surface whereas the darkest regions indicate valleys. It is observed that the membrane surface morphology has been changed upon addition of Cu-BTC particles. The higher the loadings of Cu-BTC added, the rougher the membrane surface and this can be possibly due to the particle agglomeration which occurred on membrane surface as evidenced in Figure 7.

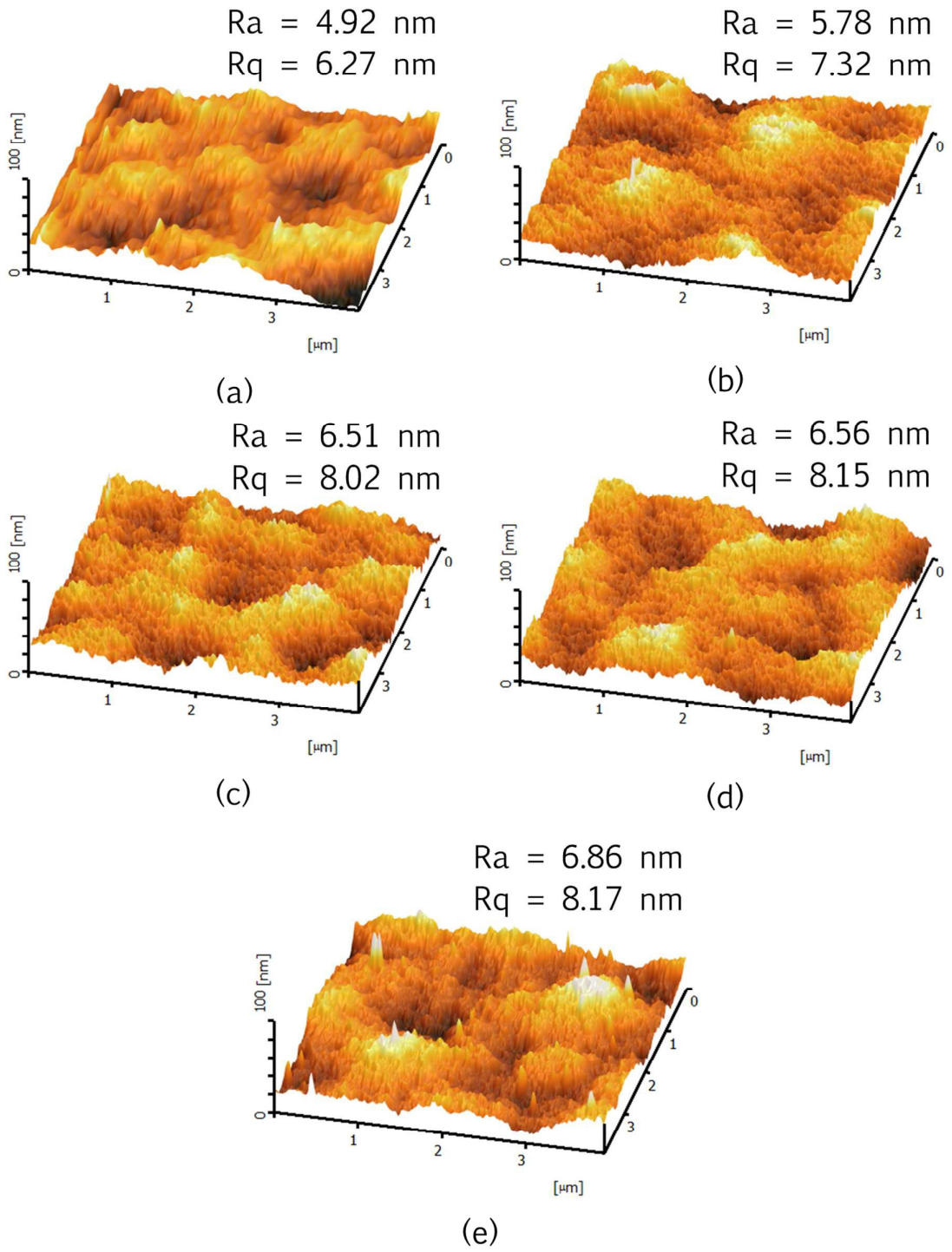

Figure 9: 3D AFM images of PPSU and PPSU/Cu-BTC membranes with their respective surface roughness values, (a) control PPSU, (b) PPSU/0.5Cu-BTC, (c) PPSU/0.8Cu-BTC, (d) PPSU/1Cu-BTC and (e) PPSU/3Cu-BTC.

3.3 Performance of asymmetric PPSU and PPSU/Cu-BTC mixed matrix membranes

The influence of Cu-BTC loading on the pure methanol flux of membrane was studied in the operating pressure ranging from 6 to 14 bar. Results from Figure 10 show that the Cu-BTC loading as well as operating pressure have a considerable influence on the methanol flux. Of the membranes studied, it is found that the PPSU/3Cu-BTC membrane always shows the highest solvent flux. Increasing Cu-BTC loading seems to be important in enhancing solvent flux of PPSU-based membrane. The greater fluxes of the PPSU/Cu-BTC membranes in comparison to the PPSU membrane can be attributed to the pores of Cu-BTC which act as solvent preferential path, facilitating the transport of the methanol through the membrane [34]. The possible surface defects due to the significant particles aggregation as shown in Figure 7(e) might also create voids that lead to greater solvent flux. To further confirm the presence of voids in the membrane made of highest Cu-BTC loading, filtration experiments using different types of dyes were carried out to determine the changes in membrane MWCO. Detailed discussion of this part will be provided in the following paragraph. Meanwhile, it is observed that with increasing the operating pressure, the solvent flux of each membrane tends to increase correspondingly. The flux enhancement is expected as higher driving force is created for methanol to permeate at higher operating pressure. The operating pressure conditions as applied in this work also reveal that all the PPSU-based membranes could withstand high operating pressure without collapsing. However, detailed mechanical analysis as shown in Figure 6 indicates PPSU/0.8CuBTC has the highest tensile strength among all the prepared membranes.

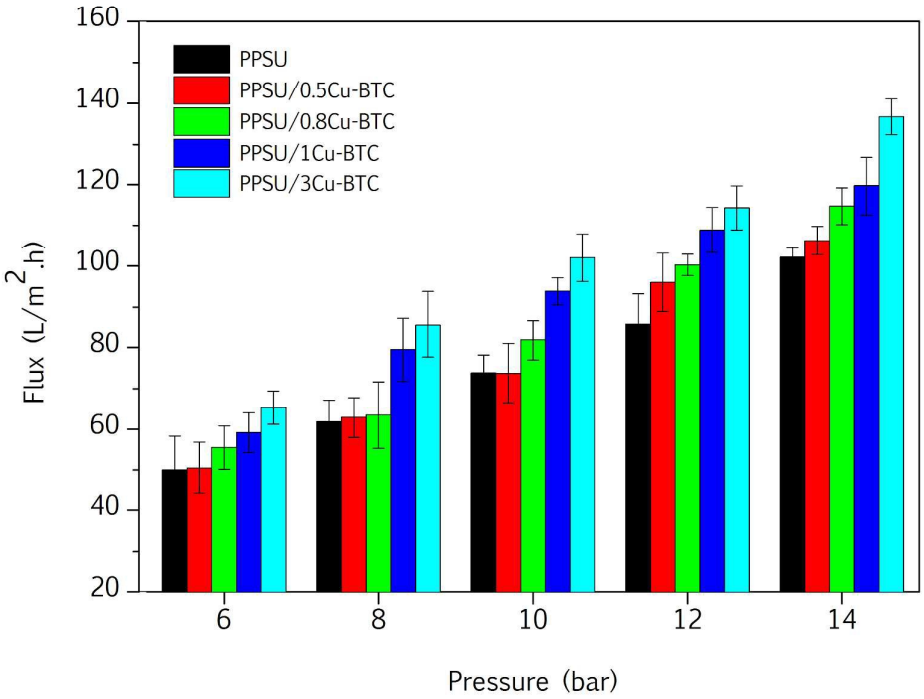

Figure 10: Methanol flux of PPSU and PPSU/Cu-BTC membranes as a function of operating pressure.

As shown in Figure 11, the rejection of dyes is plotted against their molecular weights (MWs) to determine the MWCO of the PPSU and MMMs. MWCO is determined by plotting rejection of solutes against solute MW and interpolated at solute MW with 90% rejection [16]. It can be seen that the membrane rejection is increased with increasing solute MW, irrespective of Cu-BTC loading. As the MW of the solute gets larger, the sieving effect due to steric hindrance increases and this as a result leads to higher rejection rate [9, 45, 46]. With respect to MWCO, it is reported that the membranes incorporated with 0.5–1 wt% Cu-BTC display MWCO relatively smaller than that of control membrane while highest Cu-BTC loading (i.e. 3 wt%) causes the membrane MWCO to increase significantly. The remarkable increase in MWCO (by 37% compared to control membrane) can be possibly caused by the surface defects resulted from significant particle agglomeration as discussed in earlier section. In summary, it can be said that an MMM with good combination of flux and selectivity could only be produced provided the loading of the Cu-BTC used is fixed at 0.8 wt%.

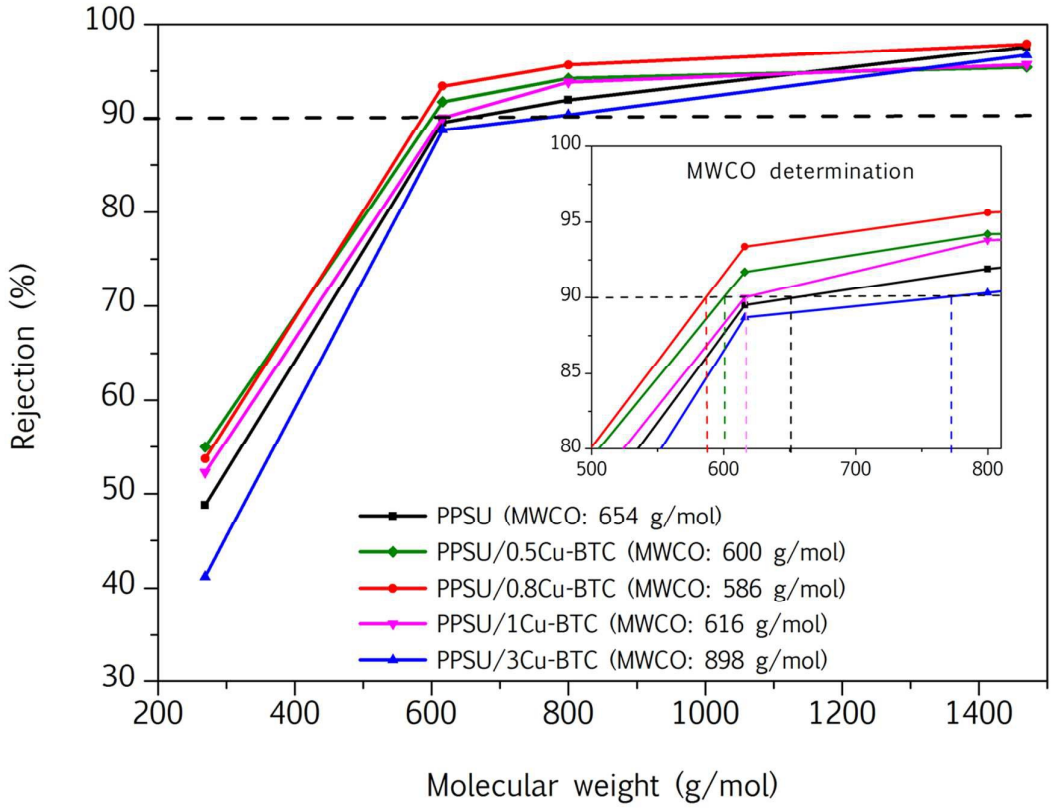

Figure 11: MWCO curves of PPSU and PPSU/Cu-BTC membranes prepared at different Cu-BTC loading.

Figure 12 shows the flux profile of the membrane with and without Cu-BTC as a function of time for pure methanol solvent at 6 bar. As can be seen, the fluxes of both membranes tend to decline at the early filtration process, but PPSU/Cu-BTC membrane achieves faster flux constant (at min-60) compared to control PPSU membrane (at min-150). The enhanced flux stability of the MMM can be due to the improved mechanical strength as Cu-BTC is an ideal filler that compatible with polymer matrix, hence strengthen the membrane structure and consequently reduces flux decline due to membrane compaction. At the end of experiment, it is reported that the PPSU/Cu-BTC membrane only suffers less than 8% flux decline in comparison to 26% as shown in the control PPSU membrane.

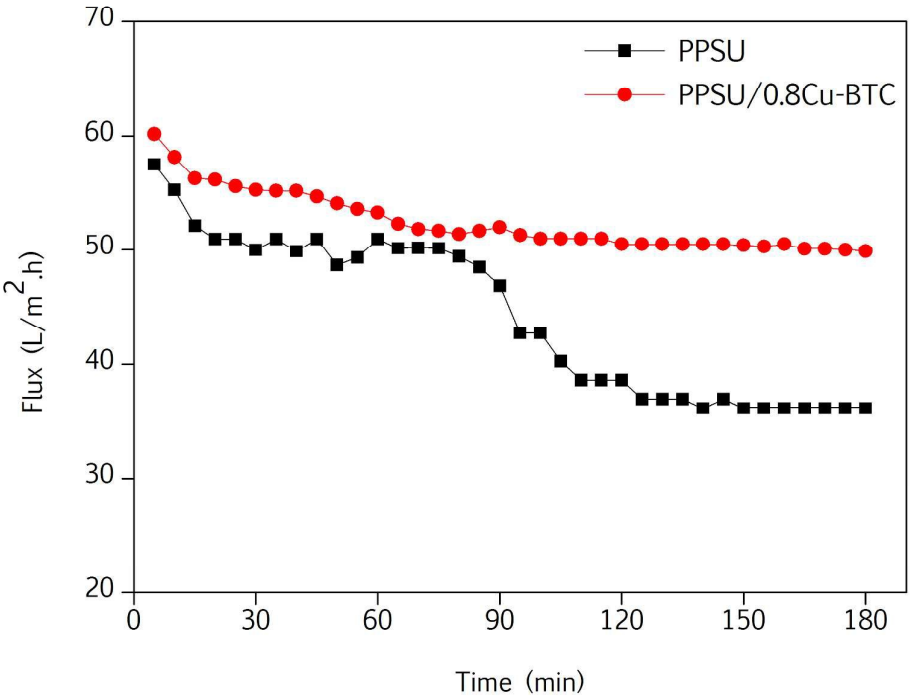

Figure 12: Flux profile of PPSU and PPSU/0.8Cu-BTC membranes.

4.0 Conclusions

MMMs containing Cu-BTC nanoparticles in PPSU matrix were successfully prepared via phase inversion process and the effects of Cu-BTC loadings on MMMs were studied with respect to structural properties and separation performance in solvent medium. Results from the membrane characterizations showed that the thermal and surface properties of MMMs were influenced by increasing the content of Cu-BTC particles in the PPSU matrix. The finger-like structure across the sub-layer of pristine PPSU membrane was suppressed when 0.8 wt% Cu-BTC loading was used. The micro-valleys on top surface of the membranes diminished at the highest Cu-BTC loading (3 wt%). The incorporation of a proper amount of Cu-BTC particles into the membranes was reported to enhance membrane methanol flux without compensating its selectivity. This is likely due to the nanoscale channels existed in the Cu-BTC that facilitate the transport of methanol while restrict the passage of solute. It was also reported that the increase in the membrane mechanical properties upon addition of Cu-BTC could improve not only the membrane flux stability but also minimize solvent flux decline during filtration process.

Acknowledgments

The authors are grateful to the Ministry of Education (MOE) for financial support of this work (Long-term Research Grant Scheme, grant no. of R.J130000-7837.4L803). N.A.A. Sani also thanks the MOE for the MyBrain15 (MyPhD) sponsorship received during her PhD studies.

Reference

1. L. S. White, Transport properties of a polyimide solvent resistant nanofiltration membrane, *J. Membr. Sci.*, 2002, **205**, 191-202.
2. L. Raman, M. Cheryan and N. Rajagopalan, Deacidification of soybean oil by membrane technology, *J. Am. Oil Chem. Soc.*, 1996, **73**, 219-224.
3. B. Tylkowski, I. Tsibranska, R. Kochanov, G. Peev and M. Giamberini, Concentration of biologically active compounds extracted from Sideritis ssp. L. by nanofiltration, *Food Bioprod. Process,* 2011, **89**, 307-314.
4. J. Geens, B. De Witte and B. Van der Bruggen, Removal of API's (Active Pharmaceutical Ingredients) from Organic Solvents by Nanofiltration, *Sep. Sci. Technol.*, 2007, **42**, 2435-2449.
5. I. Soroko and A. Livingston, Impact of TiO_2 nanoparticles on morphology and performance of crosslinked polyimide organic solvent nanofiltration (OSN) membranes, *J. Membr. Sci.*, 2009, **343**, 189-198.
6. I. Soroko, M. Sairam and A. G. Livingston, The effect of membrane formation parameters on performance of polyimide membranes for organic solvent nanofiltration (OSN). Part C. Effect of polyimide characteristics, *J. Membr. Sci.*, 2011, **381**, 172-182.
7. M. Namvar-Mahboub, M. Pakizeh and S. Davari, Preparation and characterization of UZM-5/polyamide thin film nanocomposite membrane for dewaxing solvent recovery, *J. Membr. Sci.*, 2014, **459**, 22-32.
8. J. Wang, Z. Yue, J. S. Ince and J. Economy, Preparation of nanofiltration membranes from polyacrylonitrile ultrafiltration membranes, *J. Membr. Sci.*, 2006, **286**, 333-341.
9. N. A. A. Sani, W. J. Lau and A. F. Ismail, Influence of polymer concentration in casting solution and solvent-solute-membrane interactions on performance of polyphenylsulfone (PPSU) nanofiltration membrane in alcohol solvents, *J. Polym. Eng.*, 2014, **34**, 489.
10. S. Darvishmanesh, J. C. Jansen, F. Tasselli, E. Tocci, P. Luis, J. Degrève, E. Drioli and B. Van der Bruggen, Novel polyphenylsulfone membrane for potential use in solvent nanofiltration, *J. Membr. Sci.*, 2011, **379**, 60-68.
11. L. Shao, X. Cheng, Z. Wang, J. Ma and Z. Guo, Tuning the performance of polypyrrole-based solvent-resistant composite nanofiltration membranes by optimizing polymerization conditions and incorporating graphene oxide, *J. Membr. Sci.*, 2014, **452**, 82-89.
12. P. Vandezande, L. E. M. Gevers and I. F. J. Vankelecom, Solvent resistant nanofiltration: separating on a molecular level, *Chem. Soc. Rev.*, 2008, **37**, 365-405.
13. X. Q. Cheng, Y. L. Zhang, Z. X. Wang, Z. H. Guo, Y. P. Bai and L. Shao, Recent Advances in Polymeric Solvent-Resistant Nanofiltration Membranes, *Adv. Polym. Tech.*, 2014, DOI 10.1002/adv.21455.
14. R. W. Baker, Membrane technology and applications, 2004, John Wiley.
15. K. Vanherck, P. Vandezande, S. O. Aldea and I. F. J. Vankelecom, Cross-linked polyimide membranes for solvent resistant nanofiltration in aprotic solvents, *J. Membr. Sci.*, 2008, **320**, 468-476.
16. J. C. Jansen, S. Darvishmanesh, F. Tasselli, F. Bazzarelli, P. Bernardo, E. Tocci, K. Friess, A. Randova, E. Drioli and B. Van der Bruggen, Influence of the blend composition on the

properties and separation performance of novel solvent resistant polyphenylsulfone/polyimide nanofiltration membranes, *J. Membr. Sci.*, 2013, **447**, 107-118.

17. T.-S. Chung, L. Y. Jiang, Y. Li and S. Kulprathipanja, Mixed matrix membranes (MMMs) comprising organic polymers with dispersed inorganic fillers for gas separation, *Prog. Polym. Sci.*, 2007, **32**, 483-507.
18. S. Kulprathipanja, Zeolites in Industrial Separation and Catalysis, 2010, Wiley.
19. L. E. M. Gevers, I. F. J. Vankelecom and P. A. Jacobs, Zeolite filled polydimethylsiloxane (PDMS) as an improved membrane for solvent-resistant nanofiltration (SRNF), *Chem. Commun.*, 2005, 2500-2502.
20. H. Siddique, E. Rundquist, Y. Bhole, L. G. Peeva and A. G. Livingston, Mixed matrix membranes for organic solvent nanofiltration, *J. Membr. Sci.*, 2014, **452**, 354-366.
21. Y.-R. Lee, J. Kim and W.-S. Ahn, Synthesis of metal-organic frameworks: A mini review, *Korean J. Chem. Eng.*, 2013, **30**, 1667-1680.
22. B. Zornoza, C. Tellez, J. Coronas, J. Gascon and F. Kapteijn, Metal organic framework based mixed matrix membranes: An increasingly important field of research with a large application potential, *Microporous Mesoporous Mater.*, 2013, **166**, 67-78.
23. D. Britt, D. Tranchemontagne and O. M. Yaghi, Metal-organic frameworks with high capacity and selectivity for harmful gases, *PNAS*, 2008, **105**, 11623-11627.
24. L. T. Nguyen, T. T. Nguyen, K. D. Nguyen and N. T. Phan, Metal–organic framework MOF-199 as an efficient heterogeneous catalyst for the aza-Michael reaction, *Appl. Catal. A*, 2012, **425**, 44-52.
25. O. Shekhah, J. Liu, R. A. Fischer and C. Woll, MOF thin films: existing and future applications, *Chem. Soc. Rev.*, 2011, **40**, 1081-1106.
26. E. V. Perez, K. J. Balkus Jr, J. P. Ferraris and I. H. Musselman, Mixed-matrix membranes containing MOF-5 for gas separations, *J. Membr. Sci.*, 2009, **328**, 165-173.
27. M. J. C. Ordoñez, K. J. Balkus Jr, J. P. Ferraris and I. H. Musselman, Molecular sieving realized with ZIF-8/Matrimid® mixed-matrix membranes, *J. Membr. Sci.*, 2010, **361**, 28-37.
28. Y. Li, F. Liang, H. Bux, W. Yang and J. Caro, Zeolitic imidazolate framework ZIF-7 based molecular sieve membrane for hydrogen separation, *J. Membr. Sci.*, 2010, **354**, 48-54.
29. S. S.-Y. Chui, S. M.-F. Lo, J. P. Charmant, A. G. Orpen and I. D. Williams, A chemically functionalizable nanoporous material $[Cu_3(TMA)_2(H_2O)_3]_n$, *Science*, 1999, **283**, 1148-1150.
30. P. Küsgens, M. Rose, I. Senkovska, H. Fröde, A. Henschel, S. Siegle and S. Kaskel, Characterization of metal-organic frameworks by water adsorption, *Microporous Mesoporous Mater.*, 2009, **120**, 325-330.
31. Z.-Q. Li, L.-G. Qiu, T. Xu, Y. Wu, W. Wang, Z.-Y. Wu and X. Jiang, Ultrasonic synthesis of the microporous metal–organic framework $Cu_3(BTC)_2$ at ambient temperature and pressure: An efficient and environmentally friendly method, *Mater. Lett.*, 2009, **63**, 78-80.
32. K.-J. Kim and H.-G. Ahn, The effect of pore structure of zeolite on the adsorption of VOCs and their desorption properties by microwave heating, *Microporous Mesoporous Mater.*, 2012, **152**, 78-83.
33. S. Basu, M. Maes, A. Cano-Odena, L. Alaerts, D. E. De Vos and I. F. J. Vankelecom, Solvent resistant nanofiltration (SRNF) membranes based on metal-organic frameworks, *J. Membr. Sci.*, 2009, **344**, 190-198.
34. J. Campbell, G. Szekely, R. P. Davies, D. C. Braddock and A. G. Livingston, Fabrication of hybrid polymer/metal organic framework membranes: mixed matrix membranes versus in situ growth, *J. Mater. Chem. A*, 2014, **2**, 9260-9271.
35. S. Darvishmanesh, F. Tasselli, J. C. Jansen, E. Tocci, F. Bazzarelli, P. Bernardo, P. Luis, J. Degrève, E. Drioli and B. Van der Bruggen, Preparation of solvent stable polyphenylsulfone hollow fiber nanofiltration membranes, *J. Membr. Sci.*, 2011, **384**, 89-96.
36. J. Scheirs, Compositional and Failure Analysis of Polymers: A Practical Approach, 2000, John Wiley & Sons.

37. J.-L. Zhuang, D. Ceglarek, S. Pethuraj and A. Terfort, Rapid Room-Temperature Synthesis of Metal–Organic Framework HKUST-1 Crystals in Bulk and as Oriented and Patterned Thin Films, *Adv. Funct. Mater.*, 2011, **21**, 1442-1447.
38. L. Ge, W. Zhou, V. Rudolph and Z. Zhu, Mixed matrix membranes incorporated with size-reduced Cu-BTC for improved gas separation, *J. Mater. Chem. A*, 2013, **1**, 6350-6358.
39. A. M. Díez-Pascual and A. L. Díez-Vicente, Effect of TiO_2 nanoparticles on the performance of polyphenylsulfone biomaterial for orthopaedic implants, *J. Mater. Chem. B*, 2014, **2**, 7502-7514.
40. S. Basu, A. Cano-Odena and I. F. J. Vankelecom, MOF-containing mixed-matrix membranes for CO_2/CH_4 and CO_2/N_2 binary gas mixture separations, *Sep. Purif. Technol.*, 2011, **81**, 31-40.
41. N. A. H. M. Nordin, A. F. Ismail, A. Mustafa, R. S. Murali and T. Matsuura, The impact of ZIF-8 particle size and heat treatment on CO_2/CH_4 separation using asymmetric mixed matrix membrane, *RSC Adv*, 2014, **4**, 52530-52541.
42. I. Soroko, M. P. Lopes and A. Livingston, The effect of membrane formation parameters on performance of polyimide membranes for organic solvent nanofiltration (OSN): Part A. Effect of polymer/solvent/non-solvent system choice, *J. Membr. Sci.*, 2011, **381**, 152-162.
43. Y. H. See-Toh, M. Silva and A. Livingston, Controlling molecular weight cut-off curves for highly solvent stable organic solvent nanofiltration (OSN) membranes, *J. Membr. Sci.*, 2008, **324**, 220-232.
44. S. Husain and W. J. Koros, Macrovoids in Hybrid Organic/Inorganic Hollow Fiber Membranes, *Ind. Eng. Chem. Res.*, 2009, **48**, 2372-2379.
45. C. S. Ong, W. J. Lau and A. F. Ismail, Treatment of dyeing solution by NF membrane for decolorization and salt reduction, *Desal Water Treat*, 2012, **50**, 245-253.
46. A. F. Ismail and W. J. Lau, Influence of feed conditions on the rejection of salt and dye in aqueous solution by different characteristics of hollow fiber nanofiltration membranes, *Desalin Water Treat*, 2009, **6**, 281-288.